Enhancing Wildfire Propagation Estimation with an Autonomous Aerial Agent

Constantinos Heracleous*, Panayiotis Kolios*§, and Christos G. Panayiotou*‡

***Abstract*— Accurately estimating wildfire propagation is pivotal for effective firefighting strategies and informed decision-making. This paper introduces a novel solution that harnesses an autonomous uncrewed aerial vehicle (UAV) agent with advanced sensing capabilities in conjunction with a wildfire spread model and the Ensemble Kalman Filter (EnKF) to enhance wildfire propagation estimations. By strategically guiding the UAV to specific areas ahead of the fire, it collects real-time data on fuel types and weather conditions, which are fused with available historical data to improve accuracy. The updated data are then utilized by the wildfire spread model and EnKF to provide estimations of wildfire propagation, which further improves the UAV path planning. The performance of the proposed solution is demonstrated in a simulated environment, highlighting its ability to enhance wildfire propagation estimation and improve the fire's current perimeter state estimation.**

I. Introduction

Wildfire propagation estimation is the process of predicting the future wildfire spread by considering factors such as weather, fuel characteristics, and topography alongside the fire's current state. Accurate estimation is vital for efficient firefighting, enabling precise resource allocation and reducing property damage and fatalities. Furthermore, it supports prompt evacuation efforts and contributes to quicker containment of fires, a necessity given the increasing frequency of wildfires attributed to climate change [1].

In the literature, the application of data assimilation techniques for wildfire propagation estimation is demonstrated, with a focus on the Ensemble Kalman Filter (EnKF) and its variants [2]. Early studies in [3], [4] highlighted. the importance of observational data and statistical methods in fire propagation estimation, developing a method that integrates a wildfire spread model with atmospheric models using EnKF, enhanced by real-time data from infield temperature sensors and imagery. Further advancements are discussed in [5], [6], where a data-driven simulator combining Rothermel's wildfire spread model [7] with an EnKF-based algorithm is presented. This approach effectively integrates fire perimeter observations, allowing estimation for wind and fuel parameters and current perimeter state. Similarly, in [8], the EnKF method is applied to the FARSITE model [9], demonstrating significant improvements in fire perimeter state estimation through repeated data assimilation cycles.

*Authors are with KIOS Research and Innovation Center of Excellence (KIOS CoE), §with the Department of Computer Science, ‡and with the Department of Electrical and Computer Engineering, University of Cyprus, Nicosia, 1678, Cyprus. {heracleous.constantinos, kolios.panayiotis, christosp}@ucy.ac.cy

In [10], [11] a short-term wildfire forecasting system was proposed based on Rothermel's model and Huygens' elliptical propagation method, utilizing an inverse modeling approach for fuel and wind parameter estimation, followed by forward modeling for more accurate fire perimeter forecasts. The authors in [12] introduced a hybrid estimation scheme combining state-parameter estimation with an ensemble transform Kalman filter (ETKF) and a radial basis function neural network (RBFNN). This approach optimizes fuel adjustment factors, demonstrating improved accuracy in fire propagation forecasts suitable for real-time applications. Finally, in [13], a state estimation scheme for wildfires was developed, integrating data from forecasters, static temperature sensors, and vision sensors, resulting in an enhanced approach for estimating the current perimeter state of an evolving wildfire in real-time.

The methods mentioned generally rely on periodic observations of the fire perimeter to refine estimations of the current fire state and also to provide estimates for input parameters such as fuel and wind, which can be used for forecasting fire spread. However, accurately determining these input parameters can be challenging, especially over large geographical areas. Fortunately, uncrewed aerial vehicles (UAVs), with their rapid deployment and advancing capabilities, are emerging as critical assets in wildfire management. Equipped with a diverse array of sensors, including various cameras, LIDAR, and weather sensors, UAVs offer comprehensive, real-time data on wildfires, proving instrumental for both mapping and monitoring their progress [14], [15]. Recent technological advancements in AI have further enabled UAVs to collect precise forest composition data, facilitating the creation of detailed fuel maps [16], [17]. The data gathered by UAVs can be integrated with fire spread models, enhancing the accuracy of predictions about the fire's future course and significantly improving firefighting efforts.

Motivated by these advancements, this work introduces

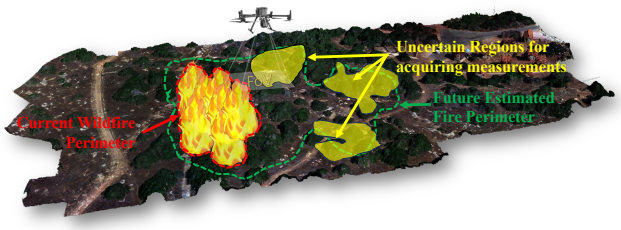

Fig. 1. The proposed solution enhances wildfire perimeter estimations by guiding the UAV to unburned uncertain regions for real-time data aquisition.

a novel approach that leverages the UAV's infield fuel and wind data measurements, combined with a wildfire spread model and EnKF, to enhance wildfire propagation estimations. The primary contributions of this work are:

- A wildfire simulator and EnKF utilizing continuously updated input data to provide, at selected intervals, estimations for the current fire perimeter state and the future fire spread over a specified estimation horizon, considering the input data value uncertainties.
- A scheme for guiding the UAV to the most uncertain regions ahead of the fire for data collection (see Fig. 1). This is achieved by generating a landscape uncertainty map after calculating the burn probability based on future fire perimeter spread estimations and combining input data uncertainty values.

The rest of this paper is organized as follows. Section II discusses the overall system model. Section III describes the problem. Section IV details the proposed solution for enhancing wildfire estimations by utilizing a UAV agent. Section V presents simulation results demonstrating the solution performance. Finally, Section VI offers some concluding remarks.

II. System Model

Let us consider the landscape where the wildfire spreads as a rectangular grid that can be mapped to $n \times m$ cells of arbitrary resolution λ adjusted to capture the spatial features adequately. The wildfire perimeter is represented by a dynamic set of 2D vertices that propagates based on the wildfire spread model described below. A UAV is deployed to gather real-time data on vegetation and weather conditions to enhance wildfire propagation estimations.

A. Wildfire Spread Model

The wildfire spread model is described by the following discrete-time nonlinear system

$$q_t = \mathcal{M}\big(q_{t-1}, \upsilon_{t-1}\big), \quad \forall t > 0, \tag{1}$$

where $q_t = [q_t^1, \dots, q_t^{N_t}]^T$ denote the wildfire perimeter at time t as a set of N_t connected fire-front vertices. Each $q_t^i = [x_t^i, y_t^i]$ represents the cartesian coordinates of the i-th fire-front vertex, while N_0 and q_0 are the initial fire-fronts amount and location, respectively. The input $\upsilon_t = [R_t, U_t, \theta_t]$ consists of matrices that represent: R the landscape's fire spread rate (m·min^{-1}), U the mid-flame wind speed (m·s^{-1}), and θ is the wind direction (rad). Specifically, $R \in \mathbb{R}^{n\times m}$ (and similarly U and θ) is a matrix of the form

$$R_t = \begin{bmatrix} R_t(1,1) & \cdots & R_t(1,m) \\ \vdots & \ddots & \vdots \\ R_t(n,1) & \cdots & R_t(n,m) \end{bmatrix}, \tag{2}$$

where each element of the matrix $R(r,c)$ denotes the rate of spread at cell (r,c) of the digitized landscape. The cell indices (r,c) correspond to the cartesian coordinates in the landscape through $r = \lceil \frac{y}{\lambda} \rceil$ and $c = \lceil \frac{x}{\lambda} \rceil$, where x and y represent the point coordinates and λ is the grid resolution. The rate of spread in each cell can be estimated using the Rothermel model from inputs known before the fire [7], [18]. These inputs are associated with documented fuel models [19]; therefore, identifying the fuel model for each cell makes it possible to estimate the rate of spread a priory. Lastly, function $\mathcal{M}(\cdot)$ in (1) consists of the dynamic model, the loop-clipping, and rediscretization algorithms that together calculate the wildfire perimeter propagation.

1) Dynamic Model: Utilizing Huygens' expansion-based approach [20] the propagation of each fire front q_t^i in the 2D plane is calculated using the following discrete-time model

$$q_t^i = q_{t-1}^i + \delta t \Delta Q_{t-1}^i, \quad \forall i = 1, \cdots, N_{t-1}, \tag{3}$$

where δt is the time step and $\Delta Q_t^i = [X_t^i, Y_t^i]$ are the orthogonal spread rate differentials

$$\begin{aligned} X_t^i &= \frac{a^2\ c\theta(\tilde{x}\ s\theta + \tilde{y}\ c\theta) - b^2\ s\theta(\tilde{x}\ c\theta - \tilde{y}\ s\theta)}{\sqrt{b^2(\tilde{x}\ c\theta - \tilde{y}\ s\theta)^2 + a^2(\tilde{x}\ s\theta + \tilde{y}\ c\theta)^2}} + c\ s\theta, \\ Y_t^i &= \frac{-a^2\ s\theta(\tilde{x}\ s\theta + \tilde{y}\ c\theta) - b^2\ c\theta(\tilde{x}\ c\theta - \tilde{y}\ s\theta)}{\sqrt{b^2(\tilde{x}\ c\theta - \tilde{y}\ s\theta)^2 + a^2(\tilde{x}\ s\theta + \tilde{y}\ c\theta)^2}} + c\ c\theta, \end{aligned} \tag{4}$$

where[1] $c\theta$ and $s\theta$ is a shortened form for $\cos\theta_t^i$ and $\sin\theta_t^i$, respectively, and θ_t^i $(0 \le \theta < 2\pi)$ is the wind direction angle that corresponds to the coordinates of q_t^i in the wind direction matrix. $\tilde{x}_t^i = x_t^{i+1} - x_t^{i-1}$ and $\tilde{y}_t^i = y_t^{i+1} - y_t^{i-1}$ denote the component differentials representing the orientation of q_t^i, while a_t^i, b_t^i and c_t^i describe the shape of an elliptical fire calculated as follows

$$a = \frac{0.5(R + \frac{R}{HB})}{LB},\ b = \frac{(R + \frac{R}{HB})}{2},\ c = b - \frac{R}{HB} \tag{5}$$

where R is the fire spread rate (m·min^{-1}) at q_t^i coordinates, ***HB*** is the head to back ratio given as $HB = \frac{LB+(LB^2-1)^{0.5}}{LB-(LB^2-1)^{0.5}}$, and ***LB*** is the length to breadth ratio given as $LB = 0.936e^{0.2566U} + 0.461e^{-0.1548U} - 0.397$, with U denoting the the mid-flame wind speed at q_t^i coordinates.

2) Loop Clipping: The dynamic model described in (3) can generate loops in the fire perimeter due to the heterogeneous fire spread rates and weather inputs [9]. To tackle this, a loop-clipping algorithm is employed that identifies intersecting segments in the perimeter and removes the responsible fire-front vertices at each time step. This process adjusts the fire-front vertices number N_t accordingly and maintains correct perimeter representation.

3) Rediscretization: The expansion of the fire perimeter causes a distance increase between adjacent fire-front vertices that affects the perimeter accuracy, particularly in highly curved sections of the perimeter. To correct this, a rediscretization algorithm has been implemented that adds new vertices by utilizing the following condition [20]

$$\max\Big(\cos\frac{\beta_t^i}{2}, \cos\frac{\beta_t^{i-1}}{2}\Big) > \Big(\frac{T_d}{\ell_t^i}\Big)^2, \tag{6}$$

[1] In (4) and in the rest of this paper, subscripts and superscripts are omitted whenever it does not lead to confusion in order to enhance clarity.

where, β_t^i is the angle formed at q_t^i between q_t^{i-1} and q_t^{i+1} vertices, and β_t^{i-1} is the angle at q_t^{i-1} between q_t^i and q_t^{i-2} vertices. Also, $\ell_t^i = \left\|q_t^i - q_t^{i-1}\right\|$ is the distance between the subsequent vertices q_t^i and q_t^{i-1}, and T_d is a positive threshold parameter. If the condition in equation (6) is true in any perimeter segment, then a new vertex is added at the midpoint of that segment (i.e., $\frac{\ell_t^i}{2}$). The algorithm runs recursively to the newly generated segment halves, and new vertices are added until the condition in (6) is satisfied in all the new perimeter segments, while the number of the fire-front vertices N_t is updated accordingly.

B. UAV Dynamics and Sensing System

The UAV can fly in 3D Cartesian space using the following discrete-time linear dynamical model for its movement

$$\chi_t = A\chi_{t-1} + Bu_{t-1}, \tag{7}$$

where $\chi_t = [p_t, \nu_t]^T$ denotes the state of the UAV at time t that consist of its position $p_t = [x_t, y_t, z_t] \in \mathbb{R}^3$ and its velocity $\nu_t = [\dot{x}_t, \dot{y}_t, \dot{z}_t] \in \mathbb{R}^3$. The input vector $u_t = [u_t^x, u_t^y, u_t^z]^T \in \mathbb{R}^3$ denotes the input force in each dimension. The matrices $A \in \mathbb{R}^{6\times6}$, $B \in \mathbb{R}^{6\times3}$ are

$$A = \begin{bmatrix} \boldsymbol{I}_{3\times3} & \delta t\boldsymbol{I}_{3\times3} \\ \mathbf{0}_{3\times3} & \rho\boldsymbol{I}_{3\times3} \end{bmatrix},\ B = \begin{bmatrix} \mathbf{0}_{3\times3} \\ \xi\boldsymbol{I}_{3\times3} \end{bmatrix}, \tag{8}$$

where δt is the time step while, $\boldsymbol{I}_{3\times3}$ and $\mathbf{0}_{3\times3}$ denote the identity matrix and zero matrix, respectively. The term $\rho \in [0, 1]$ models the air resistance, while $\xi = \frac{\delta t}{m}$ converts the input force to acceleration, with m denoting the UAV's mass.

The UAV is equipped with a weather sensor that measures wind speed and direction during flight. Mounted on its underside is a hyperspectral camera that is used to identify different fuel types that subsequently enable fire spread rate estimation [19]. The camera has a square FoV with a side length $l_t = 2z_t \tan\frac{\varphi}{2}$, where $z_t \in p_t$ is the UAV altitude, and $\varphi = 2\tan^{-1}\frac{\Upsilon}{2F}$ is the angular FoV, with Υ denoting the sensor size, and F is the lens focal length.The FoV limits in the four corner points $j = 1, \ldots, 4$ in the 2D Cartesian plane in relation to the UAV coordinates $[x_t, y_t]$ and the side length l_t, are calculated using

$$d_t^j = \left[x_t + (-1)^{j-1} \cdot \frac{l_t}{2},\ y_t + (-1)^{\left\lfloor \frac{j-1}{2} \right\rfloor} \cdot \frac{l_t}{2}\right], \tag{9}$$

which defines the coordinates of the FoV_t corners, as depicted in Fig. 2. These coordinates are then mapped to the indices in the digitized landscape using $\left\lceil \frac{d_t^j}{\lambda} \right\rceil$ providing the digitized FoV limits. Therefore, the UAV, through its onboard sensors, acquires real-time measurements for R_t, U_t, and θ_t that are inside its FoV.

III. Problem Statement

In a wildfire-affected landscape, we aim to deploy the UAV agent detailed in Sec. II. Its mission is to gather real-time data from regions ahead of the fire that have uncertain data values, with the objective of enhancing the precision of wildfire propagation estimation over a specified estimation horizon.

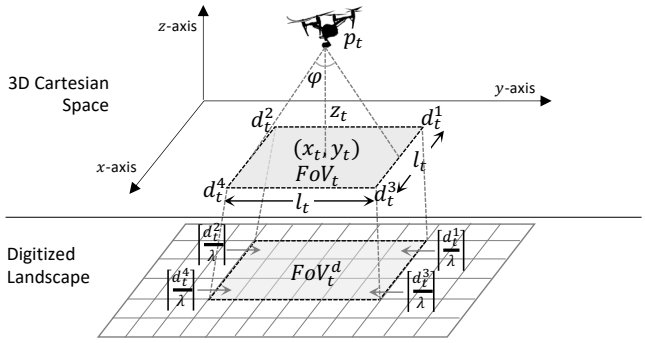

Fig. 2. UAV field of view in the cartesian space and digitized landscape.

We assume that observations of the wildfire perimeter come from a dedicated fire perimeter monitoring system, see [15], [21]. These observations are available in the form

$$q_t^o = q_t + \omega_t^o, \tag{10}$$

where $q_t^o = [q_t^{o,1}, \ldots, q_t^{o,N_t^o}]^T$ is the wildfire perimeter observation set, with N_t^o denoting its size, and each $q_t^{o,i} = [x_t^{o,i}, y_t^{o,i}]^T$. In this work, we assume that $N_t^o = N_t$. Also, $\omega_t^o \in \mathbb{R}^{2N_t^o}$ denotes zero-mean uncorrelated measurement noise with an error covariance matrix W^o, which is considered a diagonal matrix with each diagonal term representing the error variance $(\sigma^o)^2$.

Moreover, we consider any available historical data as initial value estimates for the rate of spread, wind magnitude, and wind direction, represented by matrices $R_0', U_0', \theta_0' \in \mathbb{R}^{n\times m}$, respectively. The uncertainties related to these values are captured through respective matrices $\Sigma_0^R, \Sigma_0^U, \Sigma_0^\theta \in \mathbb{R}^{n\times m}$. Within these matrices, each element (r, c) is the standard deviation, representing the uncertainty level for the corresponding cell in R_0, U_0, and θ_0.

Leveraging available observations q_t^o and input data—albeit generally imprecise—our objective is to develop a system with two primary functions. The first is to provide accurate estimates of future fire spreading patterns. This is a key insight that can help firefighters make preemptive decisions for fire suppression. The second is to strategically guide the UAV to regions that have not been burned yet but have high uncertainty with respect to the available data quality. Collecting data from those regions and feeding it back to the fire propagation model will improve the prediction accuracy of where the fire will actually move in the future.

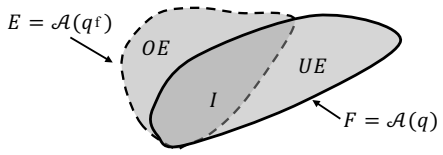

Fig. 3. Representation of the features between the true fire *F* and the estimated fire *E*, including overestimated area *OE*, underestimated area *UE*, and the intersection area *I* that used to calculate the Area Difference Index (ADI) [22].

To evaluate the performance of our proposed system, we first define the future estimated fire perimeter as a dynamic set of fire-front vertices $q^{\mathrm{f}}_{t'} = [q^{\mathrm{f},1}_{t'}, \ldots, q^{\mathrm{f},N^{\mathrm{f}}_{t'}}_{t'}]^T$, where $t' = t + \tau_H$ and τ_H is a selected estimation horizon. We then assess the accuracy of these estimations by quantifying the discrepancy between the future true wildfire perimeter $q_{t'}$ and the future estimated perimeter $q^{\mathrm{f}}_{t'}$ utilizing the Area Difference Index (ADI) [22]

$$ADI = \frac{OE + UE}{I}, \tag{11}$$

where (see Fig. 3) $OE = E - I$ denotes the overestimated area, and $UE = F - I$ denotes the underestimated area. E and F represent the estimated fire area and the true fire area, respectively, and $I = E \cap F$ is the intersection area. Lastly, $F = \mathcal{A}(q)$ and $E = \mathcal{A}(q^{\mathrm{f}})$, with function $\mathcal{A}(\cdot)$ calculating the fire area from its respective perimeter fire-front vertices.

IV. Proposed Architecture

The proposed system architecture is illustrated in Fig. 4, with an in-depth description of its interconnected components provided in the following sections.

A. Wildfire Simulator and Ensemble Kalman Filter

The wildfire simulator, together with the EnKF, provides estimates of the current and future fire perimeter states. The wildfire simulator utilizing the wildfire spread model in (1), an initial fire perimeter state and input data (i.e., $\upsilon'_t = [R'_t, U'_t, \theta'_t]$, from the data fusion scheme that is described in Sec. IV-E) generates an ensemble of n_e simulated fire perimeters with random sample errors according to the input data uncertainties. We denote the simulated fire perimeters as a set $Q^{\mathrm{s}}_t \in \mathbb{R}^{N^{\mathrm{s}}_t \times n_e}$, where the superscript s_k refers to the k-th ensemble member

$$Q^{\mathrm{s}}_t \triangleq (q^{\mathrm{s}_1}_t, \ldots, q^{\mathrm{s}_{n_e}}_t), \tag{12}$$

where each ensemble member $q^{\mathrm{s}_k}_t \in Q^{\mathrm{s}}_t$, $\forall k = 1, \cdots, n_e$ contains the 2D coordinates of $N^{\mathrm{s}_k}_t$ fire-front vertices

$$q^{\mathrm{s}_k}_t = \left[(x^{\mathrm{s}_k,1}_t, y^{\mathrm{s}_k,1}_t), \ldots, (x^{\mathrm{s}_k,N^{\mathrm{s}_k}_t}_t, y^{\mathrm{s}_k,N^{\mathrm{s}_k}_t}_t)\right]^T. \tag{13}$$

The set Q^{s}_t is then used by the EnKF with the objective to obtain estimates q^a_t of the current fire perimeter state q_t using the observations q^o_t. However, to use EnKF, it is first necessary to resize the simulated ensembles since the size $N^{\mathrm{s}_k}_t$ of each $q^{\mathrm{s}_k}_t$ can be different due to loop-clipping and rediscretization steps (see Section II-A). Therefore, each simulated perimeter $q^{\mathrm{s}_k}_t$ is interpolated in 2D to a new size

$$N^{\mathrm{s}}_t = \max\left(N^{\mathrm{s}_1}_t, \ldots, N^{\mathrm{s}_{n_e}}_t\right), \tag{14}$$

which preserves the resolution and makes all ensemble members the same size. The EnKF using the resized ensemble set Q^{s}_t, calculates the error covariance matrix $P^s_t \in \mathbb{R}^{2N^{\mathrm{s}}_t \times 2N^{\mathrm{s}}_t}$

$$P^{\mathrm{s}}_t = \sum_{k=1}^{n_e} \frac{\left(q^{\mathrm{s}_k}_t - \bar{q}^{\mathrm{s}}_t\right)\left(q^{\mathrm{s}_k}_t - \bar{q}^{\mathrm{s}}_t\right)^T}{n_e - 1}, \tag{15}$$

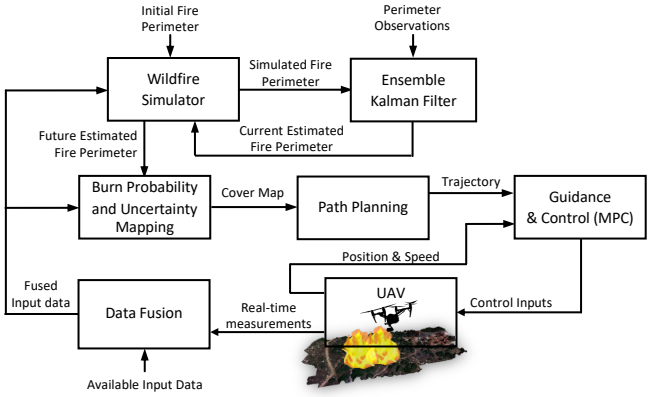

Fig. 4. Overview of the proposed system architecture

where

$$\bar{q}^{\mathrm{s}}_t \triangleq \frac{1}{n_e} \sum_{k=1}^{n_e} q^{\mathrm{s}_k}_t. \tag{16}$$

Following this, the data assimilation (or analysis) step is carried out, utilizing the observations q^o_t from (10) to update each ensemble member through the following equations

$$q^{\mathrm{a}_k}_t = q^{\mathrm{s}_k}_t + K_t\left(q^o_t + \omega^{o_k}_t - S_t(q^{\mathrm{s}_k}_t)\right) \tag{17}$$

$$K_t = P^{\mathrm{s}}_t S^T_t \left(S_t\, P^{\mathrm{s}}_t S^T_t + W^o\right)^{-1}, \tag{18}$$

where S_t is a selection operator taking 1 every $\frac{N^s_t}{N^o_t}$ fire-fronts from $q^{\mathrm{s}_k}_t$, and $\omega^{o_k}_t$ is the measurement noise and W^o its error covariance matrix. At the end of this step, the current estimated fire perimeter ensemble is generated, denoted as $Q^{\mathrm{a}}_t \in \mathbb{R}^{N^{\mathrm{a}}_t \times n_e}$

$$Q^{\mathrm{a}}_t \triangleq (q^{\mathrm{a}_1}_t, \ldots, q^{\mathrm{a}_{n_e}}_t). \tag{19}$$

The mean value of the analysis ensemble is then calculated

$$q^{\mathrm{a}}_t \triangleq \frac{1}{n_e} \sum_{k=1}^{n_e} q^{\mathrm{a}_k}_t, \tag{20}$$

which is the estimate for the current fire perimeter.

Next, the wildfire simulator using the fused input $\upsilon'_t = [R'_t, U'_t, \theta'_t]$, propagates each $q^{\mathrm{a}_k}_t \in Q^{\mathrm{a}}_t$ to a future time $t' = t + \tau_H$, generating the future fire perimeters set $Q^{\mathrm{f}}_{t'} \in \mathbb{R}^{N^{\mathrm{f}}_{t'} \times n_e}$

$$Q^{\mathrm{f}}_{t'} \triangleq (q^{\mathrm{f}_1}_{t'}, \ldots, q^{\mathrm{f}_{n_e}}_{t'}). \tag{21}$$

The mean value of the future ensemble can then be calculated after each ensemble member is resized, providing the estimated future fire perimeter at time t'

$$q^{\mathrm{f}}_{t'} \triangleq \frac{1}{n_e} \sum_{k=1}^{n_e} q^{\mathrm{f}_k}_{t'}. \tag{22}$$

The wildfire simulator and EnKF repeat the above procedure at selected time intervals, determined by various factors such as operational and computing requirements.

B. Burn Probability and Uncertainty Mapping

The goal of this component is to generate a cover map highlighting the landscape's most uncertain, unburned regions. This map will used to guide the UAV towards these areas for data collection. By utilizing the estimated future fire perimeter ensemble set $Q^{\mathrm{f}}_{t'}$ and the current estimated perimeter q^{a}_t, the burn probability $\mathcal{B}_t \in \mathbb{R}^{n\times m}$ is calculated

$$\mathcal{B}_t = \frac{1}{n_e}\sum_{k=1}^{n_e}\Big(\mathcal{O}(q^{\mathrm{f}_k}_{t'}) - \big[\mathcal{O}(q^{\mathrm{f}_k}_{t'}) \cap \mathcal{O}(q^{\mathrm{a}}_t)\big]\Big), \tag{23}$$

where each cell $\mathcal{B}_t(r,c) \in [0,1]$ depicts the probability of the cell (r,c) burning at time t'. The function $\mathcal{O}(\cdot)$ returns an $n \times m$ binary occupancy matrix according to the provided fire perimeter, i.e., fills with ones the area inside the perimeter and with zeros the area outside.

Using the uncertainty matrices for $\Sigma^R_t, \Sigma^U_t, \Sigma^\theta_t$ from the data fusion scheme (see Sec. IV-E), the uncertainty map $H_t \in \mathbb{R}^{n\times m}$ is then calculated

$$H_t = \mathcal{B}_t \times \big(w_R\Sigma^R_t + w_U\Sigma^U_t + w_\theta\Sigma^\theta_t\big), \tag{24}$$

where w_R, w_U, and w_θ are user-defined weights that adjust the relative importance of the different terms.

Finally, the binary cover map of size $n \times m$ is calculated

$$C_t(r,c) = \begin{cases} 1 & \text{if } H'_t(r,c) \geq T_{th} \\ 0 & \text{otherwise} \end{cases} \tag{25}$$

where $T_{th} = (0,1)$ is a threshold that allows the selection of uncertainty level, i.e., smaller T_{th} values will provide more number of points to be covered while larger T_{th} values will provide less number of points. Also, H'_t is the normalized version of H_t, with values scaled between 0 and 1, calculated by $H'_t = \frac{H_t - \min(H_t)}{\max(H_t) - \min(H_t)}$.

C. Path Planning

The path planning procedure employs a Traveling Salesman Problem (TSP) heuristic for calculating a reference trajectory for the UAV. Firstly, a directed graph of the landscape is generated, treating the current perimeter estimate q^{a}_t as an obstacle to ensure the UAV navigates around it. Utilizing the cover map C_t, it then identifies nodes that require coverage and the shortest paths between these node pairs are calculated. A Greedy TSP algorithm is then employed to determine the order in which to visit these nodes. The Greedy TSP starts from the node nearest to the drone's initial position and systematically progresses to the closest unvisited node until all nodes are visited. The final trajectory is obtained by concatenating the shortest paths between the visited nodes.

Finally, the procedure returns the UAV trajectory as points in 3D space by mapping the node indices to their respective X and Y Cartesian coordinates and incorporating a predetermined safe UAV altitude z_{ref}. Thus, the resultant trajectory comprises N^w waypoints, expressed as $T = [w^1, w^2, \ldots, w^{N^w}]$, where each waypoint $w^i = [x^i_w, y^i_w, z^i_{\mathrm{ref}}]$ represents the 3D Cartesian coordinates of the i-th waypoint.

D. Guidance and Control

To guide the UAV along the calculated trajectory T, we employ model predictive control (MPC). MPC's objective is to compute control inputs for the UAV over a finite prediction horizon, ensuring it traverses each waypoint of the trajectory while adhering to UAV dynamics and constraints, such as speed and acceleration. An optimization problem is formulated as follows [23]

$$\min_{u_{t+\tau-1|t}} \frac{1}{2}\sum_{\tau=0}^{N^\tau-1}\Big[(p_{t+\tau|t} - w^{\mathrm{ref}}_{t+\tau|t})^T Q (p_{t+\tau|t} - w^{\mathrm{ref}}_{t+\tau|t})\Big] \tag{26}$$

subject to $\tau \in \{0,\ldots,N_\tau - 1\}$:

$$\chi_{t+\tau|t} = A\chi_{t+\tau-1|t} + Bu_{t+\tau-1|t}, \quad \forall\tau, \tag{27}$$

$$\bar{u}_{\min} \leq u^x_{t|t}, u^y_{t|t}, u^x_{t|t} \leq \bar{u}_{\max}, \tag{28}$$

$$\bar{\nu}_{\min} \leq \dot{x}_{t|t}, \dot{y}_{t|t}, \dot{z}_{t|t} \leq \bar{\nu}_{\max}. \tag{29}$$

Equation (26) represents a quadratic cost function aiming to minimize the sum of squared tracking errors between the UAV position $p_{t+\tau|t}$ and the reference waypoint position $w^{\mathrm{ref}}_{t+\tau|t}$ over the finite prediction horizon N_τ. In (26), Q is a positive semidefinite matrix that weighs the tracking error. Equation (27) describes the UAV dynamics, detailed in Sec. II-B, where $\chi_{t+\tau|t}$ comprises the UAV position $p_{t+\tau|t}$ and velocity $\nu_{t+\tau|t}$. Vector $u_{t+\tau-1|t}$ denotes the UAV control input for each step in the horizon $\tau \in \{0,\ldots,N_\tau - 1\}$. Equations (28) and (29) impose limits on control inputs (u^x, u^y, u^z) and velocity components $(\dot{x}, \dot{y}, \dot{z})$, ensuring they stay within acceptable bounds based on UAV capabilities.

The reference waypoint w^{ref}_t in (26) is updated based on

$$\|p_t - w^{\mathrm{ref}}_t\| \leq \varepsilon, \tag{30}$$

where ε is a selected waypoint tracking error threshold. If $w^{\mathrm{ref}}_t = w^i$ at time t and the condition in (30) holds true, then in the next time step $w^{\mathrm{ref}}_{t+1} = w^{i+1}$, based on the waypoints' order in trajectory T.

E. Data Fusion

As the UAV traverses the trajectory waypoints, it gathers real-time measurements through its FoV. These measurements are integrated with existing data, updating their values and associated uncertainties through a process known as data fusion. This procedure involves continuous updates to matrices representing fire spread rate R'_t, wind magnitude U'_t, and wind direction θ'_t, along with their corresponding uncertainty matrices, i.e., Σ^R_t, Σ^U_t, Σ^θ_t. The updates are executed at each time step, according to the UAV's position and FoV. For clarity, let's consider the update process for the matrix R'_t (a similar approach applies to U'_t and θ'_t)

$$R'_t = \begin{cases} R_t(r,c), & \text{if } (r,c) \in \mathrm{FoV}^d_t \\ R'_{t-1}(r,c), & \text{otherwise.} \end{cases} \tag{31}$$

Correspondingly, the uncertainty matrix Σ^R_t (and analogously Σ^U_t and Σ^θ_t) is updated as follows:

$$\Sigma^R_t = \begin{cases} 0, & \text{if } (r,c) \in \mathrm{FoV}^d_t \\ \Sigma^R_{t-1}(r,c), & \text{otherwise.} \end{cases} \tag{32}$$

All the above matrices are initialized with the values of their corresponding available matrices R'_0, U'_0, θ'_0 and Σ_0^R, Σ_0^U, Σ_0^θ. The above process ensures that the UAV data acquisition dynamically updates the matrix values, providing enhanced inputs $\upsilon'_t = [R'_t, U'_t, \theta'_t]$ and uncertainty matrices to improve the wildfire simulator's perimeter estimations.

V. Simulation Experiments

A. Simulation Setup

The simulation experiments were conducted within the MATLAB environment to evaluate the proposed approach. The results of these simulations were derived by applying the parameter values for both the wildfire and the UAV, as outlined in Table I. To create an anisotropic fire shape, the landscape grid was partitioned into 20m by 20m squares. Within each square, the rate of spread was determined by assigning values randomly drawn from the normal distribution detailed in Table I, ensuring a diverse and realistic simulation environment for testing the proposed approach.

For the simulation experiments, historical data regarding the rate of spread R'_0, wind magnitude U'_0, and wind direction θ'_0 were randomly assigned based on their corresponding normal distributions outlined in Table I. Similarly, the uncertainty matrices Σ_0^R, Σ_0^U, and Σ_0^θ, which quantify the variability in the historical data, were determined using the standard deviation values listed in Table I for the true conditions. A total of $n_e = 150$ ensemble members (representing different fire perimeters) were initialized with a guest initial position $[1570\text{m}, 670\text{m}]$ assuming variance of 100m in both the X and Y directions. Furthermore, in the computation of the uncertainty map in (24), the weights were set as $w_R = 1$, $w_U = 0.5$, and $w_\theta = 0.5$. Finally, the prediction horizon for the MPC controller was set to $N^\tau = 10$ time steps, and the waypoint tracking error threshold was set to $\varepsilon = 30$m. These parameter values and settings were consistently applied across all simulation experiments to maintain uniformity in the evaluation process.

In this simulation setup, the proposed approach runs every 5 minutes, beginning 10 minutes after the fire starts. Hence, from $t = 10$ minutes onward, at each 5-minute interval, the system provides new fire perimeter estimations for the current time t and the future time $t' = t + \tau_H$, using the latest fused input data collected by the UAV. Concurrently, a new trajectory is recalculated at these intervals for the UAV.

Several simulation experiments were conducted, varying the uncertainty threshold values in (25) from $T_{th} = 0.1$ to 0.9, as well as testing different estimation horizon durations of $\tau_H = 20$ and 30 minutes. Additionally, to establish a benchmark, simulation experiments were performed without employing the proposed system and relying solely on the wildfire simulator and EnKF for current and future perimeter estimations using only the available historical data.

TABLE I
Simulation Parameters Values

General	
Time step: $\delta t = 1$s	Total simulation time: 80mins
Wildfire Model Parameters	
Grid size: 5km×5km	Rediscret. threshold: $T_d = 70$m
Grid resolution: $\lambda = 50$m	Initial fire-fronts: $N_0 = 30$
Rate of spread (m·min^{-1}): $R \sim \mathcal{N}(\mu_R = [0, 70], \sigma_R = [0, 80]$	Initial fire-fronts position: $q_0 = [1.5\text{km},\ 0.65\text{km}]$
Wind speed (m·s^{-1}) : $U \sim \mathcal{N}(\mu_U = 2, \sigma_U = 10)$	Wind direction (rad): $\theta \sim \mathcal{N}\big(\mu_\theta = \frac{\pi}{9}, \sigma_\theta = \frac{\pi}{9}\big)$
Observation noise: $\sigma^o = 10$m	
UAV Parameters	
Initial UAV state: $\chi_0 = [1\text{km}, 2\text{km}, 0, 0, 0, 0]$	Deploy time: 10mins
	Sensor size: $\Upsilon = 24$mm
Mass: $m = 6.5$kg	Lens focal length: $F = 24$mm
Air resistance: $\rho = 0.2$	Acceleration limits: ± 5 m·s^{-2}
Velocity limits: ± 23 m·s^{-1}	Reference altitude: $z_{\text{ref}} = 100$m

B. Simulation Results

Fig. 5 showcases snapshots[2] for every 10 minutes from a single simulation of the proposed solution, with an estimation horizon of $\tau_H = 30$ mins and an uncertainty threshold of $T_{th} = 0.3$. It captures both the current and future perimeters of the true fire alongside the estimations made by the proposed solution. Additionally, the figure illustrates the area covered by the UAV and the waypoints to be visited.

Complementing the above results, Fig. 6 provides related results for the snapshot depicted in Fig. 5(g) for $t = 70$mins. Fig. 6(a) showcases the burned probability map calculated using (23) for this particular case; and Fig. 6(b) presents the normalized uncertainty map derived using (24). Fig. 6 displays how the uncertainty map incorporates the covered areas and burn probabilities, which are then used for calculating the waypoints depicted in Fig. 5(g).

Fig. 7 examines the efficacy of the proposed solution in current fire estimation by illustrating the Area Difference Index (ADI) over consecutive estimation intervals for various uncertainty thresholds. Accompanying boxplots provide a statistical summary of the ADI values for each threshold. As a reference point, simulation results employing solely the wildfire simulator and EnKF with historical data and perimeter observations during the assimilation are labeled "Only EnKF". The proposed solution significantly enhances current fire estimations, outperforming the standard EnKF outcomes. Specifically, whereas the standard EnKF outcomes yielded a median ADI value of ≈0.24, the optimal median ADI value achieved by the proposed solution is ≈0.094 for this simulation setup.

Fig. 8 examines the performance of the proposed solution for estimating future fire propagation, showcasing the ADI values over successive estimation intervals under different

[2]A video animation of the entire simulation run is available at `https://youtu.be/lNh0nC9G22Q`.

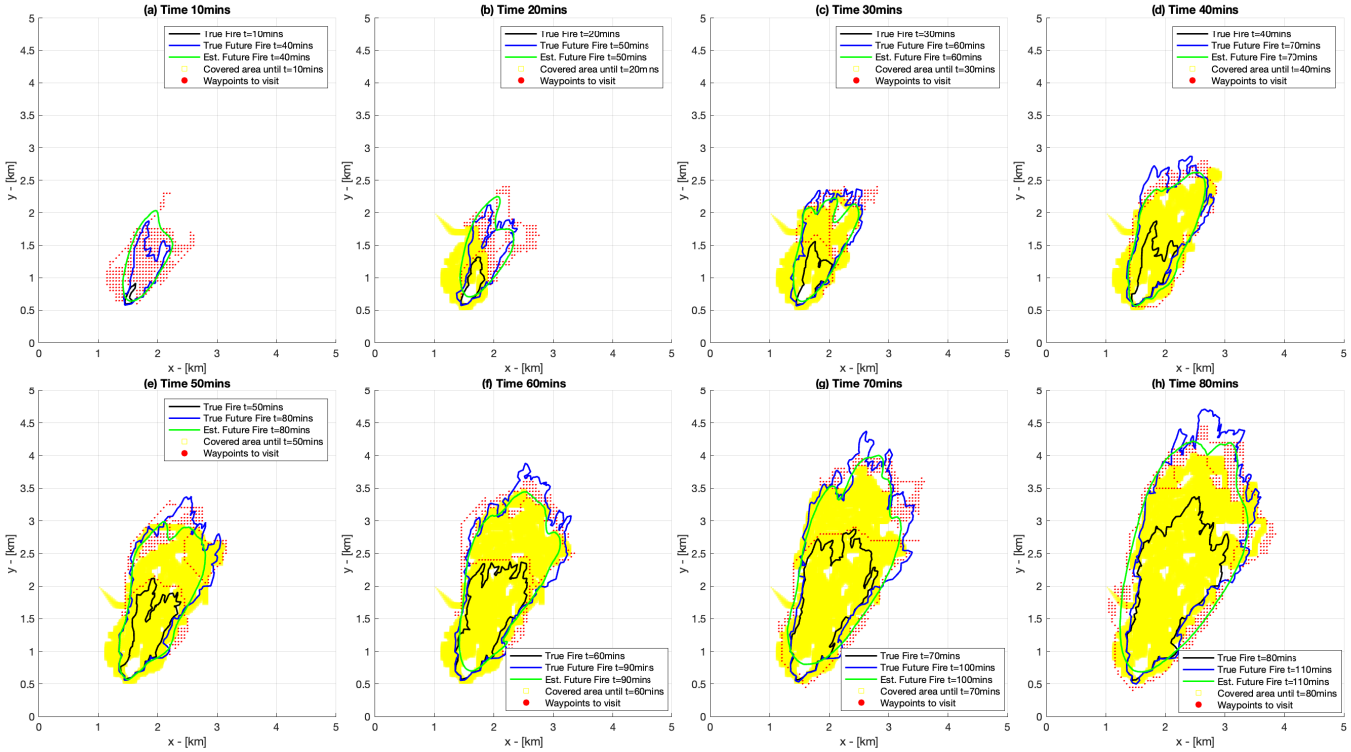

Fig. 5. Snapshots[2] from simulation of the proposed solution with selected estimation horizon $\tau_H = 30$mins and threshold $T_{th} = 0.3$ depicting at various time steps comparison between the true future fire and future fire estimation, the area covered by the UAV agent, and the calculated waypoints to be visited.

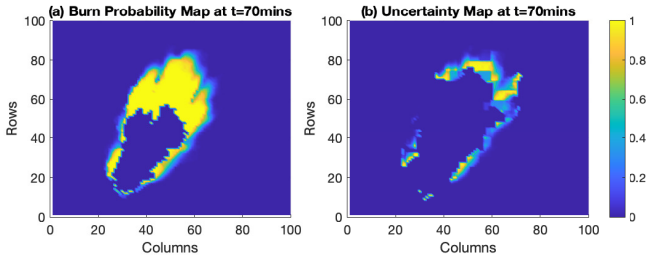

Fig. 6. Complementary to Fig. 5(g) at $t = 70$mins, showcasing: Fig.6(a) the burned probability map calculated with (23), and Fig.6(b) the normalized uncertainty map from (24).

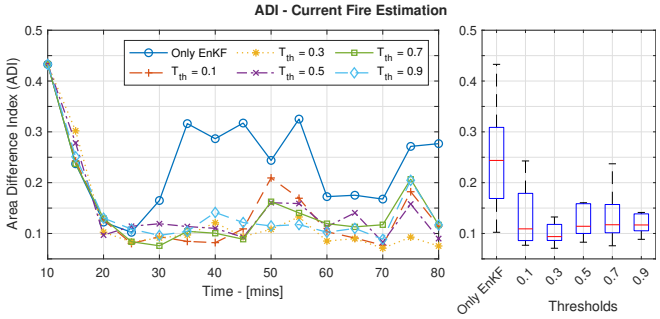

Fig. 7. Area Difference Index (ADI) values illustrate the proposed solution's performance in current fire estimation across various uncertainty thresholds over time. Boxplots summarize the ADI's statistical range for each threshold, comparing against the benchmark simulation marked as "Only EnKF".

uncertainty thresholds, supplemented by boxplots for each. Fig. 8(a) presents the results for an estimation horizon of $\tau = 20$mins, while Fig. 8(b) the results for $\tau = 30$mins horizon. The results labeled with "Only EnKF" serve as a benchmark derived by using the wildfire simulator and EnKF with the historical data and perimeter observations for estimating future fire perimeters. The results demonstrate that the proposed solution yields enhanced estimations for future fire perimeters, exceeding the benchmark results. Specifically, while the benchmark's median ADI value is $\approx$0.5, the best median ADI value obtained from the solution is $\approx$0.2, demonstrating a marked increase in accuracy for this simulation setup. The results for the $\tau = 20$ minutes horizon depicted in Fig. 8(a) show better performance over the $\tau = 30$ minutes scenario, attributed to the smaller area that the UAV needs to cover.

VI. Conclusion and Future Work

In this work, we propose a solution that leverages the sensing capabilities of a UAV along with a wildfire spread model and EnKF to enhance both current and future fire perimeter estimations. This approach directs a UAV towards unburned, uncertain areas of the landscape to collect data on fuel types and weather conditions. Through a data fusion scheme, this real-time data is combined with existing historical data, enhancing their accuracy and reducing uncertainty. The fused data are then utilized with a wildfire simulator and EnKF for computing estimations of the current fire perimeter and future fire propagation at specified intervals, which in

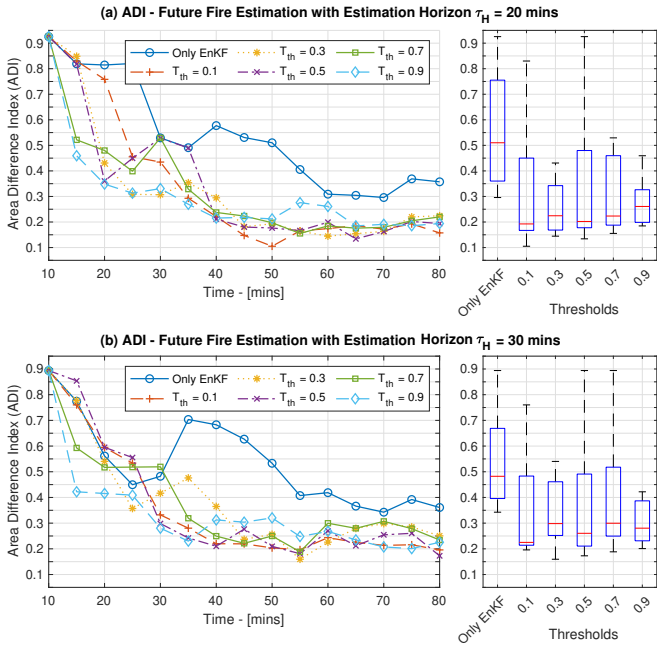

Fig. 8. ADI values for evaluating the proposed solution's performance in future fire estimation for various uncertainty thresholds accompanied with detailed boxplots for each. Fig. 8(a) presents outcomes for estimation horizon τ_H = 20mins, and Fig. 8(b) for a τ_H = 30mins horizon. Benchmark results are indicated as "Only EnKF".

turn inform updates to UAV navigation. The efficacy of our solution is demonstrated in a simulated environment, highlighting its ability to improve both current and future fire perimeter estimations.

In the future, we aim to expand the system to incorporate multiple UAVs for data collection and develop a more sophisticated path-planning algorithm that prioritizes area coverage based on uncertainty levels. Additionally, we plan to explore longer-term estimation horizons, taking into account the impact of changing weather.

ACKNOWLEDGMENT

This work has been supported by the RESTART 2016 – 2020 call for proposals for the Excellence Hubs Programme, Pillar II – Sustainable RTDI System through the Cyprus Research and Innovation Foundation under grant agreement EXCELLENCE/0421/0586 (GLIMPSE) Intelligent Multidrone Emergency Response System. It is also supported by the European Union's Horizon 2020 research and innovation program under grant agreement No 739551 (KIOS CoE - TEAMING) and from the Republic of Cyprus through the Deputy Ministry of Research, Innovation and Digital Policy.

REFERENCES

[1] United Nations Environment Programme, "Spreading like Wildfire – The Rising Threat of Extraordinary Landscape Fires," A UNEP Rapid Response Assessment, Nairobi, 2022.

[2] S. Gillijns, O. Mendoza, J. Chandrasekar, B. De Moor, D. Bernstein, and A. Ridley, "What is the ensemble Kalman filter and how well does it work?" in *2006 American Control Conference*, 2006, pp. 6 pp.–.

[3] J. Mandel, L. S. Bennethum, J. D. Beezley, J. L. Coen, C. C. Douglas, M. Kim, and A. Vodacek, "A wildland fire model with data assimilation," *Mathematics and Computers in Simulation*, vol. 79, pp. 584–606, 12 2008.

[4] J. Mandel, J. D. Beezley, J. L. Coen, and M. Kim, "Data assimilation for wildland fires," *IEEE Control Systems Magazine*, vol. 29, no. 3, pp. 47–65, 2009.

[5] M. C. Rochoux, S. Ricci, D. Lucor, B. Cuenot, and A. Trouvé, "Towards predictive data-driven simulations of wildfire spread – Part I: Reduced-cost Ensemble Kalman Filter based on a Polynomial Chaos surrogate model for parameter estimation," *Natural Hazards and Earth System Sciences*, vol. 14, no. 11, pp. 2951–2973, 2014.

[6] M. C. Rochoux, C. Emery, S. Ricci, B. Cuenot, and A. Trouvé, "Towards predictive data-driven simulations of wildfire spread Part – II: Ensemble Kalman Filter for the state estimation of a front-tracking simulator of wildfire spread," *Natural Hazards and Earth System Sciences*, vol. 15, pp. 1721–1739, 8 2015.

[7] P. L. Andrews, "The Rothermel surface fire spread model and associated developments: A comprehensive explanation," RMRS-GTR-371. Fort Collins, CO: U.S. Department of Agriculture, Forest Service, Rocky Mountain Research Station, Tech. Rep., 2018.

[8] T. Srivas, R. A. de Callafon, D. Crawl, and I. Altintas, "Data Assimilation of Wildfires with Fuel Adjustment Factors in farsite using Ensemble Kalman Filtering ," *Procedia Computer Science*, vol. 108, pp. 1572–1581, 2017.

[9] M. A. Finney, "FARSITE: Fire Area Simulator model development and evaluation," *Research Paper RMRS-RP-4 Revised*, 2004, Ogden, UT: U.S. Dept. Agric., Forest Service, Rocky Mountain Res. Station.

[10] O. Rios, W. Jahn, and G. Rein, "Forecasting wind-driven wildfires using an inverse modelling approach," *Natural Hazards and Earth System Sciences*, vol. 14, pp. 1491–1503, 6 2014.

[11] O. Rios, M. M. Valero, E. Pastor, and E. Planas, "A Data-Driven Fire Spread Simulator: Validation in Vall-llobrega's Fire," *Frontiers in Mechanical Engineering*, vol. 5, 3 2019.

[12] T. Zhou, L. Ding, J. Ji, L. Yu, and Z. Wang, "Combined estimation of fire perimeters and fuel adjustment factors in FARSITE for forecasting wildland fire propagation," *Fire Safety Journal*, vol. 116, p. 103167, 9 2020.

[13] A. Soderlund and M. Kumar, "Estimating the Spread of Wildland Fires via Evidence-Based Information Fusion," *IEEE Transactions on Control Systems Technology*, pp. 1–16, 2022.

[14] H. X. Pham, H. M. La, D. Feil-Seifer, and M. C. Deans, "A Distributed Control Framework of Multiple Unmanned Aerial Vehicles for Dynamic Wildfire Tracking," *IEEE Transactions on Systems, Man, and Cybernetics: Systems*, vol. 50, no. 4, pp. 1537–1548, 2020.

[15] C. Heracleous, P. Kolios, and C. Panayiotou, "Multi-UAV Wildfire Perimeter Monitoring System," in *2023 International Conference on Information and Communication Technologies for Disaster Management (ICT-DM)*, 2023, pp. 1–8.

[16] B. Trenčanová, V. Proença, and A. Bernardino, "Development of Semantic Maps of Vegetation Cover from UAV Images to Support Planning and Management in Fine-Grained Fire-Prone Landscapes," *Remote Sensing*, vol. 14, p. 1262, 3 2022.

[17] M. E. Andrada, D. Russell, T. Arevalo-Ramirez, W. Kuang, G. Kantor, and F. Yandun, "Mapping of potential fuel regions using uncrewed aerial vehicles for wildfire prevention," *Forests*, vol. 14, p. 1601, 8 2023.

[18] R. C. Rothmell, "A Mathematical Model for Predicting Fire Spread in Wildland Fuels," *Washington, DC, USA: Intermountain Forest Range Exp. Station, Forest Service*, vol. 115, p. 46, 1972.

[19] J. H. Scott and R. E. Burgan, "Standard fire behavior fuel models: a comprehensive set for use with Rothermel's surface fire spread model," RMRS-GTR-153. Fort Collins, CO: U.S. Department of Agriculture, Forest Service, Rocky Mountain Research Station., Tech. Rep., 2005.

[20] G. D. Richards, "An elliptical growth model of forest fire fronts and its numerical solution," *International Journal for Numerical Methods in Engineering*, vol. 30, pp. 1163–1179, 10 1990.

[21] C. Heracleous, P. Kolios, and C. G. Panayiotou, "UAV-based system for real-time wildfire perimeter propagation tracking," in *2023 31st Mediterranean Conference on Control and Automation (MED)*, 2023, pp. 13–18.

[22] T. J. Duff, D. M. Chong, and K. G. Tolhurst, "Indices for the evaluation of wildfire spread simulations using contemporaneous predictions and observations of burnt area," *Environmental Modelling & Software*, vol. 83, pp. 276–285, 2016.

[23] J. Buijs, J. Ludlage, W. V. Brempt, and B. D. Moor, "Quadratic Programming In Model Predictive Control For Large Scale Systems," *IFAC Proceedings Volumes*, vol. 35, no. 1, pp. 301–306, 2002, 15th IFAC World Congress.